Active magnetic bearing: A new step for model-free control

Jérôme de Miras, Cédric Join, Michel Fliess, Samer Riachy, Stéphane Bonnet

Active magnetic bearing: A new step for model-free control

Jérôme De Miras[a], Cédric Join[b,d,f], Michel Fliess[c,d], Samer Riachy[e,f] and Stéphane Bonnet[a]

***Abstract*— The newly introduced *model-free control* is applied to the stabilization of an active magnetic bearing, which is a most important industrial device. Experimental results are compared to those obtained via other control techniques, showing at least on-par performance with this very straightforward approach, which is moreover quite easy to implement.**

I. Introduction

Most uses of active magnetic bearings (AMB) are found in industrial applications. In particular, they find their way into high-speed rotating equipment such as turbines, machine tools, vacuum pumps or compressors. Another significant use is flywheel-based energy-storage devices, in applications ranging from satellites to biomedical equipment [6]. Indeed, magnetic bearings have many advantages over their conventional counterparts:

- Thanks to contactless, mostly frictionless operation, they can support loads with very high rotational speeds.
- Since they do not require lubrication, they are suitable for environments where excluding contamination is key, such as clean rooms, or where efficient lubrication is a problem, such as deep vacuums.

The extension of Earnshaw's theorem to magnetic forces shows it is impossible to design stable positioning systems by the mere use of permanent ferromagnetic magnets. While passive solutions based on diamanetic materials exist [23], they are uncommon in practice. This is why most applications implement active magnetic bearings (AMBs).

Active magnetic bearings are electromagnet-based and require an active control system to operate correctly [26]. They operate as follows. Each control axis (see Figure 1) features two electromagnets and a position sensor measuring rotor displacement. Each electromagnet generates a force which is proportional to the square of its coil current, and inversely proportional to the square of the air gap between its stator and the supported shaft. Through modulation of these forces, it is possible precisely position the shaft along the control axis. A centering device able to position a shaft along two degrees of freedom is obtained by combining two control axes. to completly maintain a shaft in levitation, two centering devices and a longitudinal AMB are necessary. Obviously, the nature of the forces involved introduces important nonlinearities in the physics of an axis. In addition, AMBs being very fast electromagnetic devices, major real-time constraints have to be considered when designing an appropriate control system.

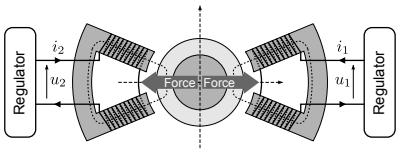

Fig. 1. An active magnetic bearing axis

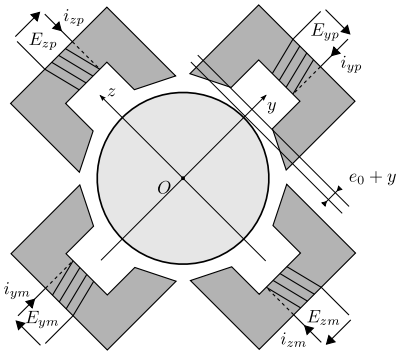

Fig. 2. Control plane with two perpendicular axis

Control of magnetic levitation systems, are the subject of numerous publications owing to their industrial importance (see e.g. [1]–[5], [10], [16], [20]–[22], [25], [28], [30]), which rely on a wide array of modern control techniques. What makes this **control problem hard** stems mainly from its complex model.

The purpose of this paper is thus to apply the new "model-free control" approach (see [11]) to that problem.[1]This control synthesis, where a "good" mathematical model becomes pointless, has already been used successfully to solve numerous control problems spanning diverse application areas (see the references in [11]). Moreover, for each real studied cases, the *ultra-local* model was of first order. Specificities of magnetic bearings – most importantly negligible friction – necessitates a second order ultra-local model. This is a major novelty.

[a]Heudiasyc (CNRS, UMR 7253), Université de Technologie de Compiègne, BP 20529, 60205 Compiègne, France. {demiras, sbonnet}@hds.utc.fr

[b]CRAN (CNRS, UMR 7039), Université de Lorraine, BP 239, 54506 Vandœuvre-lès-Nancy, France. Cedric.Join@univ-lorraine.fr

[c]LIX (CNRS, UMR 7161), École polytechnique, 91128 Palaiseau, France. Michel.Fliess@polytechnique.edu

[d]AL.I.E.N. (ALgèbre pour Identification & Estimation Numériques), 24-30 rue Lionnois, BP 60120, 54003 Nancy, France. www.alien-sas.com {cedric.join, michel.fliess}@alien-sas.com

[e]ECS-Lab (EA 3649), ENSEA, 6 avenue du Ponceau, 95014 Cergy-Pontoise, France. samer.riachy@ensea.fr

[f]Projet Non-A, INRIA Lille – Nord-Europe, France.

[1]See [9] for a first draft in French.

This paper is organized as follows. Section II sketches some basics on model-free control. Then, its application to magnetic bearings, including lab experiments and a performance comparison with two different control techniques are discussed in Section III. Finally, some insight into future developments is sketched in Section IV.

II. A short summary of model-free control[2]

A. The ultra-local model

The unknown global description of the plant is replaced by the *ultra-local model*

$$\boxed{y^{(\nu)} = F + \alpha u} \tag{1}$$

where

- the derivation order $\nu \geq 1$ is selected by the practitioner;
- $\alpha \in \mathbb{R}$ is chosen by the practitioner such that αu and $y^{(\nu)}$ are of the same magnitude.

Remark 1: Note that ν has no connection with the order of the unknown system, which may be described with distributed parameters like partial differential equations (see, for instance, [19] for hydroelectric power plants).

Remark 2: The existing examples show that ν may always be chosen quite low. In all existing concrete case-studies $\nu = 1$, with the single exception of the magnetic bearings where $\nu = 2$ since frictions are almost negligible.[3]
Some comments on F are in order:

- F is estimated via the measure of u and y;
- F subsumes not only the unknown structure of the system but also any perturbation.

B. Intelligent PIDs

Set $\nu = 2$ in Equation (1):

$$\ddot{y} = F + \alpha u \tag{2}$$

Close the loop via the *intelligent proportional-integral-derivative controller*, or *iPID*,

$$\boxed{u = -\frac{F - \ddot{y}^* + K_P e + K_I \int e + K_D \dot{e}}{\alpha}} \tag{3}$$

where

- $e = y - y^\star$ is the tracking error,
- K_P, K_I, K_D are the usual tuning gains.

Combining Equations (2) and (3) yields

$$\ddot{e} + K_D \dot{e} + K_P e + K_I \int e = 0$$

where F does not appear anymore. The tuning of K_P, K_I, K_D is therefore quite straightforward. This is a major benefit when compared to the tuning of "classic" PIDs.

[2]See [11] for more details. See [18] for the implementation on cheap and small programmable devices.

[3]See the explanation in [11].

If $K_I = 0$ we obtain the *intelligent proportional-derivative controller*, or *iPD*,

$$\boxed{u = -\frac{F - \ddot{y}^* + K_P e + K_D \dot{e}}{\alpha}} \tag{4}$$

Set now $\nu = 1$ in Equation (1):

$$\dot{y} = F + \alpha u \tag{5}$$

The loop is closed by the *intelligent proportional-integral controller*, or *iPI*,

$$u = -\frac{F - \dot{y}^* + K_P e + K_I \int e}{\alpha} \tag{6}$$

If $K_I = 0$, it yields an *intelligent proportional controller*, or *iP*,

$$u = -\frac{F - \dot{y}^* + K_P e}{\alpha} \tag{7}$$

C. Estimation of F

F in Equation (1) is assumed to be "well" approximated by a piecewise constant function F_{est}. According to the algebraic parameter identification developed in [12], [13], rewrite, if $\nu = 1$ for simplicity's sake, Equation (5) in the operational domain (see [31] for instance)

$$sY = \frac{\Phi}{s} + \alpha U + y(0)$$

where Φ is a constant. We get rid of the initial condition $y(0)$ by multiplying both sides on the left by $\frac{d}{ds}$:

$$Y + s\frac{dY}{ds} = -\frac{\Phi}{s^2} + \alpha \frac{dU}{ds}$$

Noise attenuation is achieved by multiplying both sides on the left by s^{-2}. It yields in the time domain the realtime estimate

$$F_{\text{est}}(t) = -\frac{6}{\tau^3} \int_{t-\tau}^{t} \left[(\tau - 2\sigma)y(\sigma) + \alpha\sigma(\tau - \sigma)u(\sigma)\right] d\sigma$$

where $\tau > 0$ might be quite small. This integral may of course be replaced in practice by a classic digital filter.

III. Magnetic bearings

A. A simplified model

The model used for simulations considers a single axis and is thus monovariable. Focusing on axis y (Fig. 2), the radial acceleration of the rotor can be written as

$$m\ddot{y} = F_{yp} + F_{ym} + F_p, \tag{8}$$

where F_{yp} and F_{ym} are the coil-generated magnetic forces and F_p an additive, constant disturbance such as gravity. Neglecting the effects of magnetic saturation and hysteresis, it follows

$$F_{yp} = \frac{\lambda_1 {i_{xp}}^2}{2(e_0 - y)^2} \text{ and } F_{ym} = -\frac{\lambda_2 {i_{xm}}^2}{2(e_0 + y)^2} \tag{9}$$

where e_0 is the nominal gap between the shaft and the coils and parameters λ_1 and λ_2 depend on the electromagnet and shaft geometries. Since each axis consists of two symmetrical actuators, the latter are both assumed equal to the single

parameter λ_y. Combining Equations (8) and (9), yields a model which is not linearizable at the origin – where the shaft is centered and currents are zero (see [3]). However, a model suitable for linear analysis and control design can be obtained by applying a constant premagnetisation bias current I_0 to both coils. The constant magnetic flux present in the two actuators eliminates the flux creation time, which leads to an almost linear response of the shaft for small current variations around I_0. Using a bias current has one major flaw though. Since the two coils are always active, their energy consumption is much higher. Nonlinear operation of an AMB is thus more efficient, as only one of the coils is active at any time.

In the latter operating mode, currents i_{yp} and i_{ym} are mutually exclusive and can be expressed as a function of a single virtual current i_y:

$$i_{ym} = \begin{cases} -i_y & \text{if } i_y < 0 \\ 0 & \text{otherwise} \end{cases} \quad \& \; i_{yp} = \begin{cases} i_y & \text{if } i_y > 0 \\ 0 & \text{otherwise.} \end{cases} \tag{10}$$

Equation (10) implies that either F_{yp}, or F_{ym} is 0 at any given time. Equation (9) then yields

$$F_{yp} + F_{ym} = \frac{\lambda_y \, \text{sign}(i_y) {i_y}^2}{2(e_0 - \text{sign}(i_y) y)^2}, \tag{11}$$

which gives the simulation model through substitution into Equation (8).

B. Model parameters

Values of the physical parameters m, λ_y and e_0 are given in the Tableau I. The setpoint follows a low-pass-filtered, 10-Hertz square signal. As magnetic bearings are subject to minimal damping, the chosen control law is an iPD controller (4) which is known to match a classical *PID* controller [11]. Its parameters are $K_I = 0$, $\alpha = .9$, $K_P = 14692$ and $K_D = 266$. **These values are the same as those of the nonlinear PID use for comparison in real experiment.**

In the simulation, the constant disturbance F_p changes sign at $t = .25$ s. A low amplitude noise (less than 2×10^{-6}) is added to the output. The simulation results, obtain with the simplified model and our intelligent controller given on Figures 3 and 4, show the efficacy of our string without any further tuning.

C. Experimentation

In contrast to the simulations presented above, the experiment deals with a complete bearing where all degrees of freedoms are driven simultaneously by model-free control laws.

The test-bench used for these experiments is a laboratory AMB supplied by the Swiss company MECOS-TRAXLER AG, model miniVS (Figure 5). It features a magnetic suspension unit comprising a rotor, two active centering devices and an active longitudinal bearing, whose parameters are summarized in the Tableau I.

All five control axes are driven by a single PC running real-time Simulink code. Inputs are sampled at a frequency higher than that of the control law to allow for efficient filtering. Two series low-pass filters with a time constant t_o are used to this end.

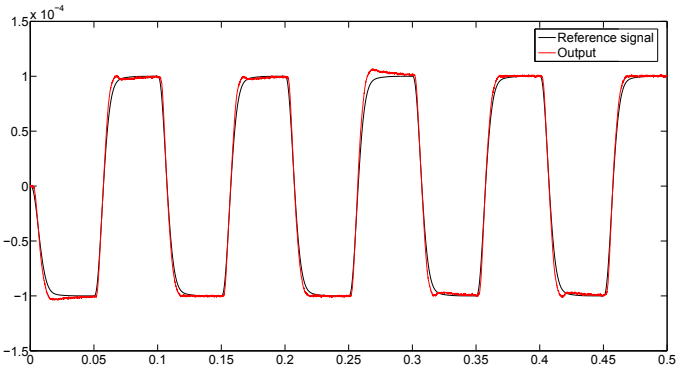

Fig. 3. Output (red) and reference (black)

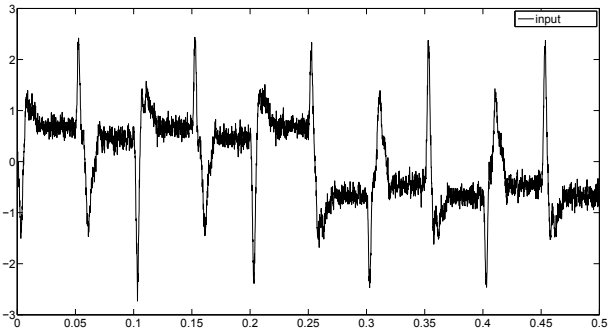

Fig. 4. Control signal u

In order to assess the performance of the model-free approach, a total of three control laws have been implemented:

- The model-free control described above. All axes are assumed to be independent.
- A global, Euler-Lagrange model-based nonlinear control law [8]. *PID* controllers are tuned to output desired values for the second derivatives of the generalized coordinates of the model according to chosen closed-loop dynamics. The third order of this closed loop is form as a product of a first order (time constant: $0.0045\,s$) and a second order (angular frequency: $180\,rd.s^{-1}$ and

TABLE I
EXPERIMENTAL AMB PARAMETERS

Parameter	Variable	Value
Rotor mass	m	$3,097\,kg$
Maximum coil current	I_{max}	$6\,A$
Nominal gap	e_0	$0,5\,10^{-3}\,m$
Coil parameter	$\lambda_{y,z}$	$2,51\,10^{-6}\,mH.m$
Acquisition period except *invMod* control	T_m	$33\,10^{-6}\,s$ $66\,10^{-6}\,s$
ADC resolution		$12 - bit$
ADC measurement range		$0,5\,10^{-3}\,m$
Input numeric filter time constant	t_o	$1\,10^{-3}\,s$
Control laws period	T_e	$132\,10^{-6}\,s$

Fig. 5. The test-bench.

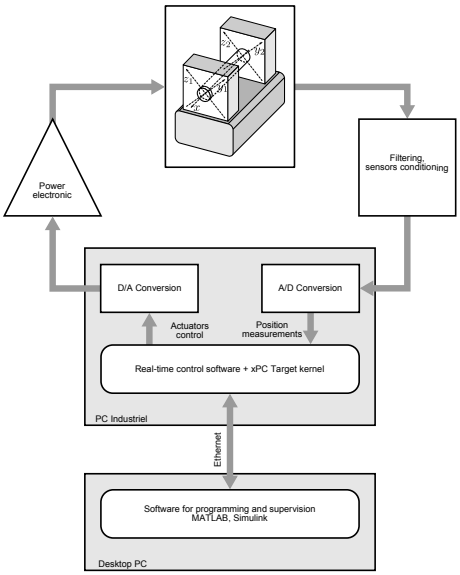

Fig. 6. Overview of the control system

damping factor: 1.1). Full model equations are then used to compute the matching currents to apply to the plant.

- A discrete nonlinear controller [2] where desired currents are obtained through a table-based numerical inversion of the behavior of an axis as a function of the desired shaft position at the next time stepp.

Let y_1, z_1 and y_2, z_2 be the positions of the shaft ends. y_1, z_1 and the x axis are kept at the nominal gap by an *iPD* controller. y_2 is made to follow a square reference signal varying from zero to $e_0/8$ at a frequency of 2 Hz. Likewise, z_2 is made to follow a sinusoidal reference signal varying from $-e_0/8$ to $e_0/8$ at the same frequency. Authors chose this reference signal as good indicators to to interpret the performance of control laws. Both y and z axes are subject to a perturbation due to gravity, while the x axis is to be

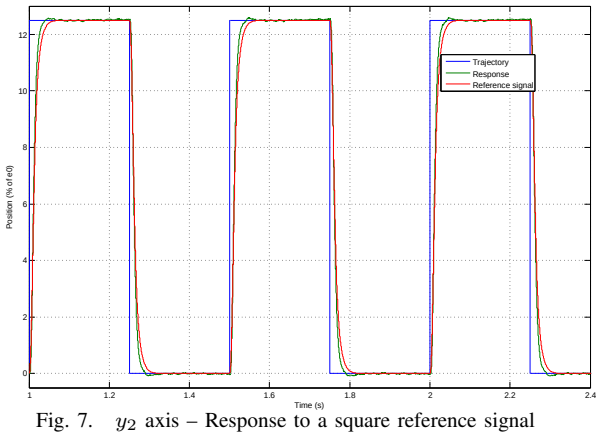

Fig. 7. y_2 axis – Response to a square reference signal

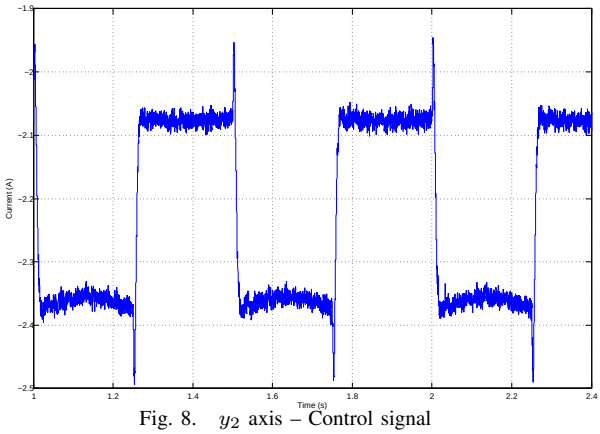

Fig. 8. y_2 axis – Control signal

stabilized close to the nonlinearizable origin of the model[4].

As shown on Figures 13 and 14, keeping the x-axis at the origin is hard as it is the point where the coil currents are zero. The time needed to establish a current in each coil induces a slight delay that prevents instantaneous reaction from the controller. In contrast, this phenomenon does not occur on the y and z axes since a nonzero current is always flowing through the coils to oppose gravity.

Figure 7 shows the value of the y_2-axis position, featuring both the reference square signal and a desired output signal obtained through low-pass filtering of the former. The matching control signal is shown on Figure 8. A significant noise level can be observed as the input filter does not completely cancel measurement noises and the derivative term *D* of the controller is a rough approximation.

The control signal itself is shaped by the combined influence of three elements:

- Since both y and z axes are directed towards the ground, negatives currents are needed to compensate for gravity.
- The value of the current necessary to compensate for gravity is $-2.07\,A$ for the nominal gapp.

[4]As the table on which the test-bench resides is not perfectly horizontal, this axis still experiences some gravity. This explains the non-zero average of the control signal shown on Figure 14

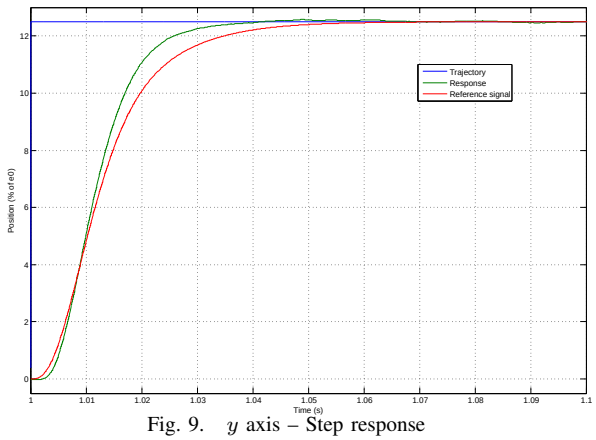

Fig. 9. y axis – Step response

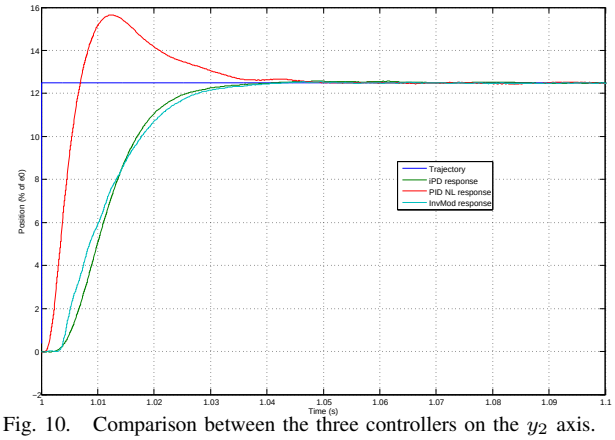

Fig. 10. Comparison between the three controllers on the y_2 axis.

- The offset relative to the nominal gapp. In the experiment, the rotors moves away from the electromagnet which maintains its position. Hence, the current has to increase with the gap to keep the magnitude of the force opposing gravity. The model error estimator $\hat{F}$ perfectly fulfills its function and compensates for this nonlinearity.

Figure 9 details a single step response of the y_2-axis. The system response is slightly ahead of the reference signal $y_2^\star$ it should be following. Indeed, $\hat{F}$ compensates for errors between the real system and that on which the control law is based with a slight delay. This phenomenon also depends on the value of the α parameter, here 2.0[5] for both the y and z axes.

Figure 10 details a single step response of the y_2-axis of all three control laws. They all have been tuned to feature the same response time.

Compared to the nonlinear global *PID* control, the model-free controller also eliminates the steady state error due to gravity but without any overshoot. Its behavior is also almost indistinguishable from that of the model inversion-based controller. Moreover, it achieves this result with a much lighter computing cost, keeping in mind the model inversion-based controller had been giving the best results on this test-bench until the present experimentation.

Figures 11 and 12 show the z_2 axis response to its sinusoidal reference and the matching control signal. The results are again correct as expected.

Finally, Figures 13 and 14 show the stabilization performance of the controller for the x axis and the associated control signal. The high frequency content of the control signal is the result of the noise generated by the derivative approximation use in the PI function with a little sampling period and minimum interval measurement of positions (see Table I).

Figure 13 also shows the response of the model inversion-based controller, which yields a tighter stabilization of the shaft at the origin, which is nonlinearizable in the model as explained before. Since at this point the impact of the

[5]The difference with the value used in simulations is due to a heavier real system

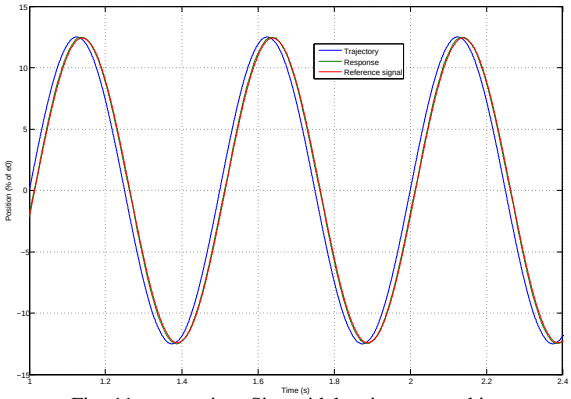

Fig. 11. z_2 axis – Sinusoidal trajectory tracking

nonlinearity on currents is at its highest, it is hard to define an optimal value for the α coefficient of the emphiPD controller in this case. Event if the model inversion-based controller better captures that nonlinearity, stabilization is still achieved by the model-free controller, albeit a larger noise.

IV. Conclusion

The model-free control synthesis

- yields as good results as the nonlinear *PID*,[6]

[6]The difference is that the PID has not filtered reference of the step signal of the input.

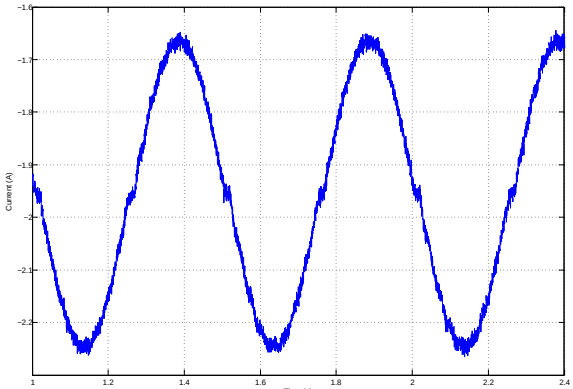

Fig. 12. z_2 axis – Control signal

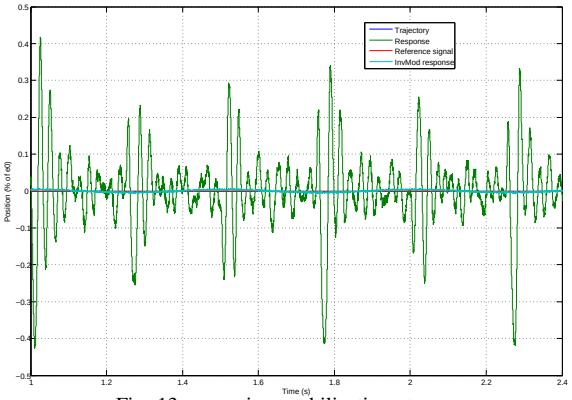

Fig. 13. x axis – stabilization at zero

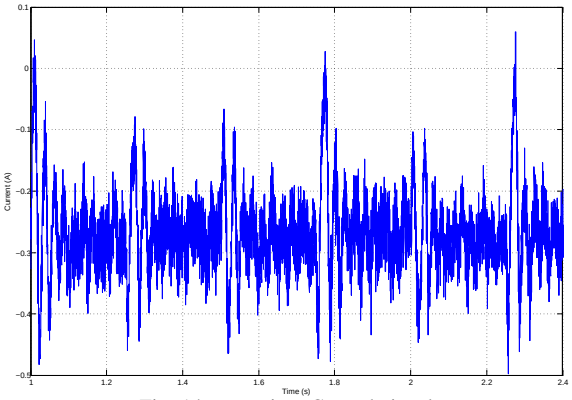

Fig. 14. x axis – Control signal

- matches the laboratory benchmark model inversion-based controller with a much lower computing cost than the two other control laws.

Still, the level of noise obtained when trying to stabilize the shaft at a point where the current is 0 and the model is nonlinearisable shows a tight coupling between the quality of the results and the numerical value of the parameter α. It indicates a possible path towards improvements of our approach. As the proposed control scheme is not directly connected to the AMB model, it remains valid as well for this type of devices at different scales contrarily to other control systems.

REFERENCES

[1] H.M.N.K. Balini, C.W. Scherer, J. Witte (2010). Performance enhancement for amb systems using unstable H_∞ controllers. *IEEE Trans. Control Syst. Techno.*, vol. 19, pp. 1479–1492.

[2] S. Bonnet, J. De Miras, B. Vidolov (2008). Nonlinear one-step predictive control of an active magnetic bearing. *17^{th} IFAC World Congress*, Seoul.

[3] A. Charara, J. De Miras, B. Caron (1996). Non-linear control of a magnetic levitation system without premagnetization. *IEEE Trans. Control Syst. Techno.*, vol. 4, pp. 513–523.

[4] S. Chen (2011). Robust nonlinear smooth feedback control of a three-pole active magnetic bearing system. *IEEE Trans. Control Syst. Techno.*, vol. 19, pp. 615–621.

[5] S.-Y. Chen, F.-J. Lin (2011). Robust nonsingular terminal sliding-mode control for nonlinear magnetic bearing system. *IEEE Trans. Control Syst. Techno.*, vol. 19, pp. 636–643.

[6] A. Chiba, D.G. Dorrell, T. Fukao, O. Ichikawa, M. Oshima, M. Takemoto (2005). *Magnetic Bearings and Bearingless Drives*. Elsevier.

[7] D. Cho, Y. Kato, D. Spilman (1993). Sliding mode and classical controllers in magnetic levitation systems. *IEEE Control Systems Magaz.*, vol. 13, pp. 42–48.

[8] J. De Miras, A. Charara (1998). A vector oriented control for a magnetically levitated shaft. *IEEE Trans. Magnetics*, vol. 34, pp. 2039–2041.

[9] J. De Miras, S. Riachy, M. Fliess, C. Join, S. Bonnet (2012). Vers une commande sans modèle d'un palier magnétique. *7^e Conf. Internat. Francoph. Automatique*, Grenoble. Accessible at `http://hal.archives-ouvertes.fr/hal-00682762/en/`

[10] H. Du, N. Zhang, J.C. Ji, W. Gao (2010). Robust fuzzy control of an active magnetic bearing subject to voltage saturation. *IEEE Trans. Control Syst. Techno.*, vol. 18, pp. 164–169.

[11] M. Fliess, C. Join (2013). Model-free control. *Int. J. Control*, DOI: 10.1080/00207179.2013.810345. Accessible at `http://hal.archives-ouvertes.fr/hal-00828135/en/`

[12] M. Fliess, H Sira-Ramírez (2003). An algebraic framework for linear identification. *ESAIM Control Optimiz. Calc. Variat.*, vol. 9, pp. 151–168.

[13] M. Fliess, H. Sira-Ramírez (2008). Closed-loop parametric identification for continuous-time linear systems via new algebraic techniques. in eds. H. Garnier and L. Wang, *Identification of Continuous-time Models from Sampled Data*. Springer, pp. 362–391.

[14] M. Fujita, F. Matsumara, M. Shimizu (1990). H^∞ robust control design for a magnetic suspension system. *2^{nd} Int. Sympp. Magnetic Bearings*, Tokyo.

[15] W. Grega, A. Pilat (2005). Comparison of linear control methods for an amb system. *Int. J. Appl. Math. Comput. Sci.*, vol. 15, pp. 245–255.

[16] T.R. Grochmal, A.F. Lynch (2007). Control precision tracking of a rotating shaft with magnetic bearings by nonlinear decoupled disturbance observers. *IEEE Trans. Control Syst. Techno.*, vol. 15, pp. 1112–1121.

[17] J. Huang, L. Wang, Y. Huang (2007). Continuous time model predictive control for a magnetic bearing system. *PIERS Online*, vol. 3, pp. 202–208.

[18] C. Join, F. Chaxel, M. Fliess (2013). "Intelligent" controllers on cheap and small programmable devices. *2^{nd} Int. Conf. Control Fault-Tolerant Systems*, Nice. Accessible at `http://hal.archives-ouvertes.fr/hal-00845795/en/`

[19] C. Join, G. Robert, M. Fliess (2010). Vers une commande sans modèle pour aménagements hydroélectriques en cascade. *6^e Conf. Internat. Francoph. Automat.*, Nancy. Accessible at `http://hal.archives-ouvertes.fr/inria-00460912/en/`

[20] M.S. Kang, W.H. Yoon (2006). Acceleration feedforward control in active magnetic bearing system subject to base motion by filtered-x lms algorithm. *IEEE Trans. Control Syst. Techno.*, vol. 14, pp. 134–140.

[21] J. Lévine, J. Lottin, J.-C. Ponsart (1996). A nonlinear approach to the control of magnetic bearings. *IEEE Trans. Control Syst. Techno.*, vol. 4, pp. 524–544.

[22] F. Mazenc, M. S. de Queiroz, M. Malisoff, F. Gao (2006). Further results on active magnetic bearing control with input saturation. *IEEE Trans. Control Syst. Techno.*, vol. 14, pp. 914–919.

[23] R. Moser, J. Sandtner, H. Bleuler (2001). Diamagnetic suspension system for small rotors. *J. Micromechatronics*, vol. 1, pp. 131–137.

[24] K. Nonami, H. Yamaguchi (1994). μ-synthesis of a flexible rotor magnetic bearing system. *4^{th} Int. Sympp. Magnetic Bearings*, Zurich.

[25] M.S. de Queiroz, S. Pradhananga (2007). Control of magnetic levitation systems with reduced steady-state power losses. *IEEE Trans. Control Syst. Techno.*, vol. 15, pp. 1096–1102.

[26] G. Schweitzer, H. Bleuler, A. Traxler (1994). *Active Magnetic Bearings*. VDF Hochschulverlag.

[27] H.F. Steffani, W. Hofmann, B. Cebulski (1998). A controller for a magnetic bearing using the dynamic programming of Bellman. *6^{th} Internat. Symp. Magnetic Bearings*, MIT, Cambridge, MA.

[28] N. Van Dijk, E. Van De Wouw, N. Doppenberg, H. Oosterling, H. Nijmeijer (2010). Robust active chatter control in the high-speed milling process. *Amer. Control Conf.*, Baltimore.

[29] B. Vidolov, C. Melin, J. De Miras, A. Charara (1996). Two-rules-based fuzzy logic control and sliding mode control of an active magnetic bearing. *5^{th} Int. Conf. Fuzzy Systems*, New Orleans.

[30] K. Youcef-Toumi, S. Reddy (1992). Dynamic analysis and control of high speed and high precision active magnetic bearing. *J. Dyn. Sys. Meas. Control.*, vol. 114, pp. 623–633.

[31] K. Yosida (1984). *Operational Calculus* (translated from the Japanese). Springer.